# Independent Analysis of Seismicity and Rockfall Scenarios for the Yucca Mountain Repository

M.J. Apted
Monitor Scientific
3900 S. Wadsworth Blvd., Denver, CO 80235
USA

J.M. Kemeny
University of Arizona
Dept. Mining and Geological Engineering, Tucson, AZ 85721
USA

C.D. Martin
University of Alberta
Dept. Civil and Environmental Engineering, Edmonton, AB T6G 2W2
Canada

R.J. James
Anatech Corp.
5435 Oberlin Dr., San Diego, CA 92121
USA

## ABSTRACT

Yucca Mountain is located in the somewhat seismically active Basin and Range province. Future seismic activity is identified by the US Nuclear Regulatory Commission and the US National Academy of Sciences as a key scenario for safety assessment of a proposed repository at Yucca Mountain. As part of its on-going program of conducting independent analyses of scientific and technical issues that could be important to the licensing of the Yucca Mountain repository, EPRI has conducted an analysis of the combined scenarios of seismic activity and stability of emplacement drifts with respect to the long-term repository safety. In this paper we present the results of 3D finite element simulations of both static and dynamic loading of a degraded waste package. For the static case, the expected maximum static load is determined by utilizing relationships between cave height and the bulking factor. A static load representing 30 meters of broken rock was simulated using the finite element model. For the dynamic case, block size and velocity data from the most recent Drift Degradation AMR are used. Based on this, a rock block with a volume of 3.11 $m^3$ and with an impact velocity of 4.81 m/s was simulated using the finite element model. In both cases, the results indicate that the waste package remains intact.

## INTRODUCTION

Over the past 18 months the Electric Power Research Institute (EPRI) has assembled a rockfall team to analyze the occurrence and consequences of rockfall in the emplacement drifts in the Yucca Mountain repository. The purpose of this study is to develop an independent perspective and safety analysis of the combined issues of seismic activity and stability of emplacement drifts for a repository at Yucca Mountain. Previously, EPRI has conducted independent analyses of key safety assessment issues regarding a repository at Yucca Mountain (EPRI, 2004a). Recent EPRI reports have included assessment of the speculative formation of deliquescent brines (EPRI, 2004b), extrusive release of radionuclides from a potential future igneous event intersecting a repository (EPRI, 2004c), and release of radionuclides

following a potential future intrusive igneous event intersecting a repository (EPRI, 2005a). This present study is the latest contribution to this series of independent EPRI reviews, and focuses on (1) seismic analysis and (2) rockfall analysis for the planned Yucca Mountain repository.

"Rockfall" is the term used here for the movement and dislodging of rock blocks in the underground drifts at the proposed YM repository. The emplacement drifts in the YM repository will be excavated using a tunnel-boring machine and will be cylindrical in shape, with a diameter of 5.5 meters. The proposed Yucca Mountain repository is to be located in volcanic tuff at depths ranging from 250 to 350 meters. In general there is expected to be a large variation in the strength of the rock mass, from medium-weak in the areas of the repository where there is a high density of lithophysae, to medium-strong in the non-lithophysal zones. 85% of the repository will be in the weaker lithophysal zones and 15% of the repository will be in the stronger non-lithophysal zones.

Here we consider the behavior of the repository for one million years. In this time frame there are four primary drivers for rockfall in the underground drifts, as described below:

1. Thermally-induced rockfall. The storage of high-level radioactive waste (HLW) will result in temperatures up to 160$^{o}$ C at the walls of the underground drifts. This will result in thermal stresses, which could either increase or decrease the likelihood of rockfall. The peak of the thermal pulse will be about 80 years after closure, with higher-than-ambient temperatures that continue for over 5000 years.
2. Seismically-induced rockfall from an earthquake. A number of earthquakes with peak ground velocities (PGV) over 1 m/s are predicted to occur in the $10^6$-year time frame. Studies around the world have shown that earthquakes with a PGV over 1 m/s can result in rockfall in underground drifts.
3. Seismically-induced rockfall from an igneous event. A magmatic dike intrusion through the repository is possible, albeit very unlikely, within the $10^6$-year time frame. Cracking of rock at the tip of an ascending dike will produce a seismic event that could result in rockfall as discussed above.
4. Time-dependent drift degradation. Over the time frame of $10^6$ years, there are a number of coupled mechanical/ hydrologic/ thermal/ chemical processes that will result in the gradual degradation of the rock mass at YM. Stress corrosion cracking[1] in the rock mass is the chief time-dependent mechanism. Stress corrosion cracking will result in a decrease in the cohesion of the rock around the drifts, potentially increasing the likelihood of rockfall.

It should be noted that the four processes described above are not independent, and that rockfall may be enhanced (or decreased) due to a combination of these processes. For instance, time-dependent drift degradation increases the likelihood of rockfall during a seismic event. Thus a large earthquake at 500,000 years may result in more rockfall than an earthquake at 10,000 years. On the other hand, thermally induced stresses decrease the likelihood of rockfall in the non-lithophysal rock. Thus a large earthquake during the peak of the thermal pulse may produce less rockfall in the non-lith than the same earthquake after the thermal pulse.

Rockfall is important because it may impact the ability of the repository to isolate nuclear waste. The potential impacts of rockfall on repository performance are listed below:

[1] The term stress corrosion cracking is used in both metal corrosion studies and rock mechanics. The two must be distinguished by the subject of the section in which the term occurs.

1. Dynamic effects of rockfall on the drip shield and/or waste package (DS/WP). A rock block that dislodges from the roof or wall of the drift will impact either the DS or the WP with a certain amount of energy or momentum. The impact energy and the result of this impact depend on the size and shape of the rock block, the velocity of impact, the size of the impact on the DS/WP, and the condition of the DS/WP at the time of the impact.
2. Static effects of rockfall on the DS/WP. If only a small amount of rockfall occurs at a location in the repository, the rock blocks may fall onto the DS/WP and then fall to the side, resulting in no long-term static loading. On the other hand, if a large amount of rockfall occurs, it will result in a permanent static load on the DS/WP. This could result in premature failure of the DS/WP due to stress corrosion and creep mechanisms.
3. Other static effects of rockfall. A significant amount of rockfall could fill parts of the drift with rock fragments. This could impact repository performance in several ways. Early rockfall (during the thermal period of the first several thousand years after repository closure) could modify the thermal characteristics in drifts by reducing the convective heat loss from waste packages due to insulation properties of the fallen rock. In addition, any rockfall has the potential to impact ventilation flow patterns within the drifts and magma flow into and within the drifts in the case of a dike intrusion through the repository (NRC, 2005).
4. Changes in seepage due to changes in the geometry of the drifts. The dislodging of rock blocks from the roof and walls of the underground drifts will change the geometry of the drifts. The drifts may enlarge in size and the surface will become rougher. This may alter the seepage characteristics and the ability of fluids to contact the DS/WP.

There are several quantitative ways to assess the amount of rockfall that occurs under various conditions. Rockfall generally results in the dislodging of individual blocks, and one measure of rockfall is the information on the blocks that dislodge under various conditions, including the size, weight, shape, and velocity of the blocks. The total amount of rockfall that occurs under various conditions is another measure. This is often reported as the total $m^3$ of rockfall per meter of drift. A final set of measures includes the stress and strain distributions (either static or dynamic) that will result on various parts of the DS/WP due to rockfall. It should be noted that this last measure depends on the material properties and geometry of the DS/WP in addition to the characteristics of the rock blocks.

Even though a number of rockfall related studies have been conducted by EPRI in the past 18 months, this paper will only discuss a subset of these topics. In particular, this paper will focus on likely bounds in the static and dynamic rock forces that could impact the DS/WP, and 3D finite element simulations analyzing the consequences of these forces. For the static case, bounds on the static force are determined by estimating a bulking factor for the broken rock at Yucca Mountain. For the dynamic case, bounds on the size and velocity of the dislodged blocks are determined utilizing modeling results from the latest Drift Degradation AMR (BSC, 2004b). The analysis of the consequence of rockfall on the WP is conducted using the 3D finite element code ABAQUS (Abaqus, 2005).

## BULKING FACTOR AND THE MAXIMUM STATIC LOAD ON THE DS/WP

The rock mass around a nuclear waste repository will be subjected to induced stresses created by a combination of the excavation response caused by the construction of the repository, the heat from the emplaced waste, and seismicity. The stress loading of the repository under these conditions will create stress paths that will result in both unloading and loading conditions, as well as stress rotation. Hence, when assessing the rock mechanics design issues associated with these conditions, two general rock mechanics modes of failure are encountered, 1) structurally controlled gravity-driven failure, and 2) stress-induced slabbing type failure. Structurally controlled failure is prevalent at shallow depths, i.e., low in-situ stress magnitudes, and slabbing failure is commonly observed at great depth, in high in-situ stress magnitudes. However, mining and tunneling experience shows that these failure processes can be

found at essentially any depth. One of the consequences of both structurally controlled and stress-induced failure process is dilation, i.e., an increase in volume. This is a well-known process that occurs in most geomaterials. Even the slip along a rough fracture will involve dilation at low to moderate stress. This dilatational process is sometimes referred to as "bulking" or "swelling" of the rock mass. Hence, failure around an underground opening that involves bulking can only continue until the tunnel becomes filled with fractured rock. The process of bulking therefore limits the rockfall consequences in an open drift. Here bulking factors are used to estimate the maximum depth of failure around a drift.

Bulking factors for various materials can be found in any excavation handbook. Bulking factors for rock are typically in the range from 1.33 to 1.60, as described in Church (1981), Blyth & De Freitas (1990), Bell & Stacey, (1992), Whittaker & Reddish (1993), and others.

It has been suggested (Gute et al., 2003) that the bulking process that will be occurring at Yucca Mountain could extend to great distances above the repository, possibly even to the surface, forming a sinkhole. There have been extensive studies that have documented the development of sinkholes. Sinkholes typically develop above mined-out stopes that were never backfilled. In all cases, sinkhole development is a shallow phenomenon. Table I, taken from Singh & Dhar (1997), shows the typical mining depths that create sinkholes. As shown in Table I, the maximum documented depth for a sinkhole is 90 meters, compared with the 250-350 meter depth at Yucca Mountain.

Table I. Mining Depth for Cases in which Sinkhole Subsidence is Reported (after Singh & Dhar (1997).

| | Location | Maximum depth (m) |
|---|---|---|
| 1 | Western Pennsylvania | 47.7 |
| 2 | Hanna Area, Wyoming | 73.2 |
| 3 | Sheridan Area, Wyoming | 77.0 |
| 4 | Beulan Area, North Dakota | 24.4 |
| 5 | Illinois Coal Basin | 50.3 |
| 6 | St David Area, Illinois | 50.3 |
| 7 | Colorado Springs Area | 45.7 |
| 8 | Superior, Wyoming | 30.5 |
| 9 | Rock Springs, Wyoming | 101.5 |
| 10 | Glenrock, Wyoming | 30.5 |
| 11 | Handidhua and Deulbera mines | 40.0 |
| 12 | Humberside & Lincolnshire | 90.0 |
| 13 | Mithapur Colliery, India | 25.0 |
| 14 | Jamuna and Kotma Area, India | 43.0 |

Palchik (2002) conducted a study of the height of caved zones over abandoned subsurface coalmines in Donetsk, Ukraine. Based on this study, Palchik (2002) developed a model that shows that the height of the caved zone (H) in bedded rocks is dependent upon the working height of underground coal extraction (h) and a bulking factor (Bf) and can be expressed as:

$$\frac{H}{h} = \frac{1}{B_f - 1} \qquad \text{(Eq. 1)}$$

Using this equation the height of the cave zone at Yucca Mountain can be estimated. The DOE's Yucca Mountain Project has used a UDEC code to model the progressive failure and bulking of emplacement drifts, with the conclusion that a bulking factor of 1.19 is appropriate to the design geometry and host-rock characteristics of their repository (BSC, 2004b). We consider this value to be conservative since it is well below the expected range discussed above. We consider the expected value for the bulking factor to be somewhere between 1.2 and 1.4. Using a bulking factor ranging from 1.2 to 1.4 in Equation (1), the maximum height of the cave zone above the roof of the original tunnel will range from 1.5 to 4 times the height of the drift. In the repository, the tunnels are partially filled (approximately one-third filled with the WP, invert, DS pallet and other parts of the EBS). Hence the maximum height of the caved zone will be significantly less than 1.5 to 4 times the height of the drift, since 1/3 of the tunnel is already filled by waste package.

Overall, the results described above indicate that caving to the surface will not occur at Yucca Mountain, and for a bound on the static load on the DS/WP that could occur, a maximum cave height of 4 times the height of the drift can be used. For the 5.5 meter diameter emplacement drifts, a caved zone 4 times the height of the drift translates to 22 meters of broken rock. In the next section a 3D finite element simulation is made using a load equivalent to a 30 m high column of rock.

## STATIC EFFECT OF ROCKFALL ON THE DS/WP

An analysis is performed to evaluate the resistance of a degraded waste package to the static overburden load due to collapse of the emplacement drift. Conservatively, it is assumed for this analysis that a large seismic event occurs at such a time that the drip shield is either missing or is in such a deteriorated state that it offers no resistance to static rock-mass loading. As a further conservatism, the Alloy 22 outer canister and lids are removed to simulate a completely eroded state, and the bare stainless steel inner canister is subjected to an increasing downward load that represents a build-up of rock rubble.

The components of the support pallet are assumed to be rigid. Displacement boundary conditions are used to simulate the narrow strips of contact between the support pallet saddles and the exterior surface of the waste package.

This analysis considers the structural response of degraded waste containers due to static loads from rubble that would pile up on top of the waste container from a chimney-type collapse of a portion of the emplacement drift. Again, no credit is taken for the drip shield. In addition, only a bare stainless steel inner canister is considered as the last structural barrier for protecting the spent fuel. The load is determined using a density of 162 pounds/ft$^3$ (2600 kg/m$^3$) for the rock and for a drift collapse that covers at least the entire waste container. The weight of rock is applied as a vertical only load over the entire length of the package and extending over about a 120° arc on the top half. Thus, no horizontal loading or confinement effects are included from rock that may be piled along the sides of the container. This is considered quite conservative since any lateral confinement would increase the strength of the container to the vertical "squashing" load. Displacement boundary conditions are applied at the support locations with the conservative assumption that the supporting structure will be rigid under this loading. The analysis is conducted using the ABAQUS 3D finite element model (Abaqus, 2005).

Fig. 1 presents contours for the maximum principal stress and for the equivalent plastic strain at a load equivalent to 30m of rock rubble on top of the waste package. This figure provides a good summary of the findings. The bare stainless steel canister with its end closures remains linear elastic for drift collapse or degradation with up to 30-m of rubble. For a 30-m high pile of rubble, points on the inner surface at the

support locations are just reaching initial yield. Note that the plastic strain is still below the 0.2% level where the yield stress is defined. Also note that the local deformations at the support locations are exaggerated somewhat in this analysis from the assumption that the support skid structure will be rigid.

It is concluded that the waste packages can easily survive the static loads that could develop from a collapse of the emplacement drift. Since the bare stainless steel canister will remain linear elastic for 30m of rubble, it is extrapolated that a waste package with all or part of the Alloy 22 protective canister present (pristine or partially degraded) will also remain linear for 30 m of rubble. While the outer canister has a higher r/t ratio (radius of curvature to thickness ratio), it will be supported by the inner structural canister, and it also has a much higher yield strength. Thus, a 30-m column of rock far exceeds the possible load that can be developed in degraded drifts due to rockfall and bulking.

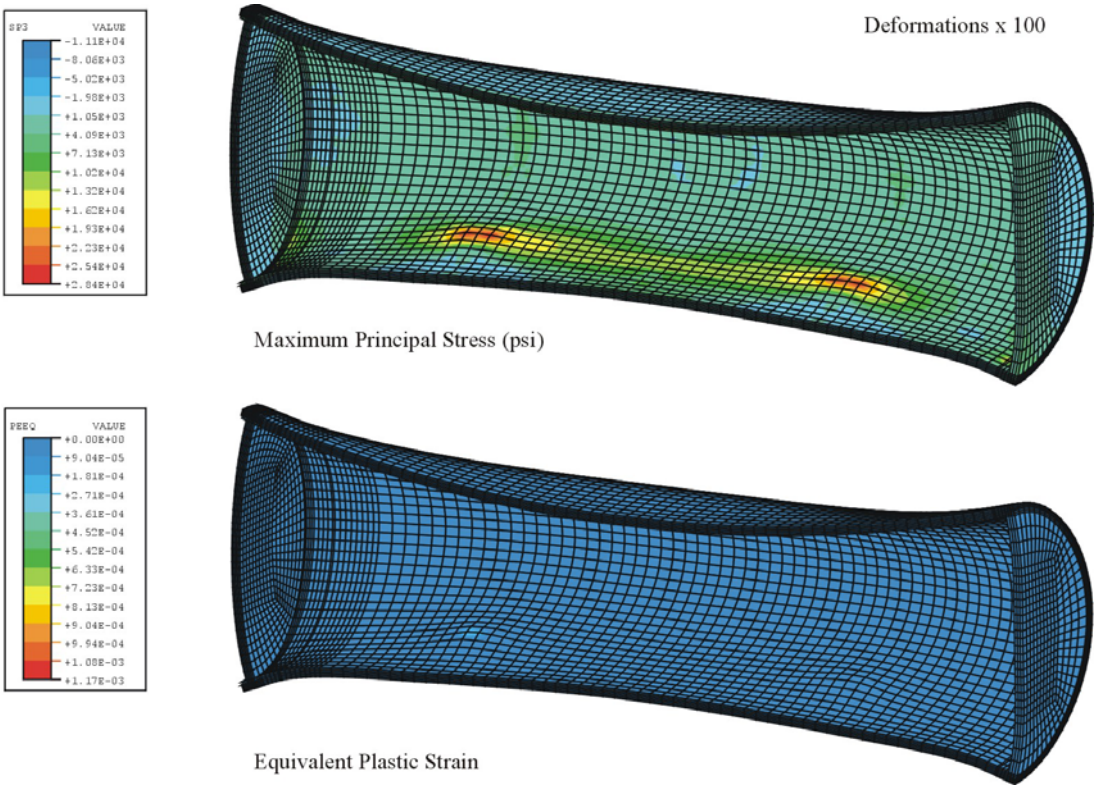


Fig. 1. Static response of degraded waste package to 30 m high pile of rubble

## LARGEST ROCK BLOCKS DISLODGED DUE TO A SEISMIC EVENT

The rock mass in the repository horizon at Yucca Mountain can be generalized into two distinct rock types, the lithophysal units and the non-lithophysal units. In the non-lithophysal units, the rock mass consists of very competent intact rock separated by discontinuities. The discontinuities consist of joints and vapor-phase partings. Due to the stochastic nature of the discontinuities, rock blocks formed by the intersection of discontinuities can range in volume from $cm^3$ to up to 10 $m^3$. The lithophysal units are weaker due to the presence of lithophysal voids. The variability in the rock mass strength in the lithophysal units depends on the lithophysal porosity, which ranges from 5 to 40%. Both the strength and the Young's modulus for the rock mass varies with lithophysal porosity, with unconfined compressive

strength varying from 2 to 35 MPa, and the rock mass Young's modulus varying from 2 to 20 GPa. Rock blocks in the lithophysal units are formed by cracks connecting neighboring lithophysae, with block volumes expected to be less than 0.1 $m^3$. Therefore, for the purpose of determining the biggest and highest momentum blocks that could impact the DS/WP, only rockfall in the non-lithophysal units are considered here.

Table II. a) Details on 50 3DEC Simulations for Rockfall in Non-lithophysal Unit Due to Seismic Events with PGV Between 1 and 4 m/s (source: BSC, 2004b), b)15 Seismic Sets used in the 50 3DEC Simulations Described in Table IIa (BSC, 2004b, Table X-2).

*Reported numbers are PGV (cm/s). H1 and H2 are the two horizontal ground motions and V is the vertical ground motion.*

| Case | Ground Motion Set | Fracture Pattern | Number of rockfall | Max Block Size (m^3) | Total Rockfall Volume (m^3) |
|---|---|---|---|---|---|
| 14 | 7 | 22 | 24 | 0.25933 | 1.844114 |
| 15 | 11 | 21 | 27 | 2.4933 | 7.0666 |
| 16 | 11 | 30 | 60 | 0.28457 | 4.263971 |
| 17 | 16 | 27 | 1 | 0.044715 | 0.044715 |
| 18 | 14 | 26 | 17 | 0.15877 | 0.543965 |
| 19 | 13 | 10 | 75 | 0.87439 | 7.374617 |
| 20 | 5 | 19 | 13 | 0.090018 | 0.4173 |
| 21 | 10 | 9 | 10 | 0.46684 | 1.040874 |
| 22 | 5 | 23 | 20 | 0.299 | 1.8461 |
| 23 | 12 | 5 | 30 | 1.3463 | 5.217497 |
| 24 | 3 | 6 | 14 | 0.29272 | 1.308361 |
| 25 | 3 | 17 | 79 | 2.7811 | 14.29615 |
| 27 | 6 | 14 | 23 | 3.7045 | 5.661104 |
| 28 | 7 | 25 | 27 | 0.64993 | 3.519735 |
| 29 | 13 | 3 | 16 | 0.37505 | 1.385953 |
| 31 | 16 | 79 | 2 | 0.12259 | 0.148625 |
| 32 | 12 | 7 | 2 | 0.18051 | 0.192814 |
| 33 | 1 | 102 | 10 | 0.37038 | 0.725063 |
| 34 | 16 | 75 | 36 | 0.52073 | 2.844848 |
| 35 | 11 | 33 | 10 | 0.52442 | 1.449465 |
| 36 | 5 | 78 | 35 | 0.62041 | 2.696764 |
| 38 | 3 | 29 | 173 | 3.5275 | 42.02974 |
| 39 | 5 | 37 | 54 | 1.3377 | 8.178643 |
| 40 | 6 | 99 | 46 | 7.9057 | 21.90231 |
| 41 | 16 | 42 | 22 | 0.31433 | 2.14505 |
| 42 | 6 | 24 | 4 | 0.061251 | 0.110552 |
| 43 | 4 | 59 | 55 | 0.89396 | 6.231508 |
| 44 | 9 | 65 | 94 | 1.4034 | 8.815078 |
| 45 | 10 | 39 | 14 | 0.83942 | 2.489211 |
| 46 | 6 | 50 | 15 | 0.41744 | 0.891036 |
| 48 | 16 | 35 | 7 | 0.092381 | 0.275758 |
| 49 | 5 | 57 | 182 | 6.0535 | 24.09928 |
| 50 | 9 | 67 | 39 | 1.2478 | 5.812328 |
| 51 | 10 | 63 | 9 | 0.60388 | 1.055593 |
| 52 | 9 | 82 | 99 | 1.3926 | 15.87992 |
| 53 | 12 | 4 | 26 | 3.031 | 4.524856 |
| 54 | 1 | 83 | 22 | 2.0552 | 6.371107 |
| 55 | 12 | 16 | 19 | 0.26465 | 1.284638 |
| 56 | 3 | 98 | 60 | 0.9414 | 6.055578 |
| 57 | 14 | 28 | 32 | 0.19568 | 1.434695 |
| 58 | 4 | 8 | 3 | 0.10436 | 0.132964 |
| 59 | 2 | 74 | 38 | 0.30994 | 2.129925 |
| 60 | 11 | 80 | 11 | 0.12925 | 0.526277 |
| 61 | 12 | 81 | 6 | 0.06776 | 0.298893 |
| 62 | 12 | 71 | 10 | 1.2676 | 1.806721 |
| 63 | 11 | 96 | 0 | 0 | 0 |
| 64 | 14 | 49 | 94 | 1.2166 | 13.61141 |
| 65 | 7 | 20 | 37 | 0.3676 | 3.020488 |
| 66 | 3 | 62 | 39 | 0.54907 | 2.775588 |
| 67 | 9 | 41 | 26 | 3.695 | 7.60142 |

| Ground Motion Set | H1 | H2 | V |
|---|---|---|---|
| 1 | 104.58 | 83.31 | 70.88 |
| 2 | 104.58 | 125.02 | 145.25 |
| 3 | 104.58 | 262.05 | 398.11 |
| 4 | 104.59 | 100.41 | 152.27 |
| 5 | 104.58 | 166.71 | 106.52 |
| 6 | 104.54 | 45.61 | 173.88 |
| 7 | 104.51 | 89.33 | 333.16 |
| 8 | 104.56 | 152.20 | 98.16 |
| 9 | 104.59 | 357.76 | 281.76 |
| 10 | 104.60 | 31.81 | 50.16 |
| 11 | 104.60 | 126.04 | 120.31 |
| 12 | 104.54 | 70.34 | 100.60 |
| 13 | 104.58 | 103.75 | 318.01 |
| 14 | 104.62 | 40.87 | 92.78 |
| 16 | 104.56 | 67.43 | 137.53 |

The size and characteristics of the largest blocks expected to impact the DS/WP due to a seismic events with PGVs ranging from 1 to 4 m/s has been extracted from the most recent Drift Degradation AMR (BSC, 2004b).

For the non-lithophysal rock, the analysis of rockfall due to seismic events with PGVs between 1 and 4 m/s is based on 50 simulations made using the 3DEC computer program. Details of the 50 simulations are given in Tables IIa and IIb. Table IIa gives the ground motion set number and the fracture pattern number associated with each of the 50 simulations. 15 ground motion sets were considered, as shown in Table IIb. The PGA for these 15 sets varied from 1 to 4 m/s, and 105 fracture pattern sets were

considered. A 100 m x 100 m x 100 m fracture model was first constructed using the FRACMAN computer program based on the actual Yucca Mountain fracture statistics. These were used to identify 105 submodels each with a size of 25 m x 25 m x 25 m to be picked from the large model. A full description of these results is given in the Drift Degradation AMR (BSC, 2004b).

Each of the 50 simulations modeled 25 meters of drift. In total, therefore, 1250 meters of drift were simulated. It is estimated that about 10 km of drift in the Yucca Mountain repository are in the non-lithophysal units, and therefore the total amount of rockfall that will be expected in the non-lith will be about 8 times what is predicted with the 50 simulations. In total, 1767 blocks were dislodged in the 50 simulations representing a total rockfall volume of about 255 $m^3$. To put this number in perspective, the amount of volume in the 1250 meters of drift available for rockfall is about 20,000 meters (taking out the volume occupied by the DS/WP). Thus the total rockfall accounts for only about 1% of the available drift volume. This assumes that the 1250 meters of drift only encountered a single seismic event with a range in PGV from 1 to 4 m/s. It also does not take into account any time-dependent degradation in the rock material properties. It also does not take into account multiple seismic events The worst rockfall occurred for simulation number 38, with about 42 $m^3$ of rockfall over the 25 m length of drift. Even in this worst case, the rockfall represents only about 11% of the available drift volume. It should also be remembered that the PGV used for the 50 simulations ranged from 1 to 4 m/s, whereas EPRI considers that the maximum possible PGV for Yucca Mountain is only 2 m/s (EPRI, 2005c). If this lower value were used, the amount of anticipated rockfall would be further reduced. For example, excluding the simulations in Table 9-1 using ground motion sets with PGV's exceeding 2 m/s (sets 3, 7, 9 and 13 in Table 9-2) results in simulation number 40 (PGV of 1.7 m/s) showing the greatest volume of rockfall of 22 $m^3$. This value is approximately half of the peak rockfall volume indicated for all of the simulations run using a PGV of up to 4 m/s (Simulation 38).

The individual block volumes in the rockfall from the 50 simulations ranged from 0.01 to 8 $m^3$. The largest blocks are of interest to repository performance, since these blocks have the potential to damage the DS/WP and result in premature failure of the DS/WP. Table III lists the 30 rock blocks with the highest impact momentum, along with information on block volume, mass, velocity, momentum and energy. Table III also lists information on their location of impact and impact angle. Table III shows that the most hazardous blocks have volumes between 1 and 8 $m^3$ and velocities of 1 to 7 m/s.

Table III. The 25 Rock Blocks with the Highest Impact Momentum from the 50 Simulations Shown in Table II. (BSC, 2004b)

*All reported velocities are m/s and impact locations are in meters relative to the top center of the WP.*

| volume (m^3) | x-velocity | y-velocity | z-velocity | x-imp | y-imp | z-imp | mass (metric ton) | velocity (m/s) | impact angle# | impact momentum (kg*m/sec) | impact energy (J) |
|---|---|---|---|---|---|---|---|---|---|---|---|
| 7.91E+00 | 3.21E-01 | -6.73E+00 | 4.28E-01 | -7.34E+00 | 1.16E+00 | -6.24E-01 | 19.07 | 6.76 | 118 | 128812 | 435077 |
| 3.11E+00 | 4.00E-02 | -4.77E+00 | 5.74E-01 | -6.63E+00 | 1.44E+00 | -1.27E+00 | 7.49 | 4.81 | 131 | 36017 | 86559 |
| 3.03E+00 | 4.20E-01 | -4.74E+00 | -5.22E-01 | 3.52E+00 | 1.44E+00 | -1.27E+00 | 7.31 | 4.78 | 131 | 34967 | 83622 |
| 2.85E+00 | 7.63E-02 | -4.92E+00 | 3.76E-01 | -5.47E+00 | 1.43E+00 | 1.26E+00 | 6.86 | 4.93 | 49 | 33855 | 83491 |
| 6.05E+00 | -1.70E-03 | -1.93E+00 | 9.13E-02 | -2.73E+00 | 1.43E+00 | 1.03E+00 | 14.60 | 1.93 | 54 | 28166 | 27167 |
| 1.81E+00 | 1.21E-01 | -5.16E+00 | 3.62E-02 | 6.93E+00 | 1.41E+00 | 1.25E+00 | 4.36 | 5.16 | 48 | 22516 | 58103 |
| 1.80E+00 | 9.22E-02 | -3.94E+00 | -8.98E-01 | -1.95E+00 | 1.33E+00 | 1.23E+00 | 4.35 | 4.04 | 47 | 17589 | 35552 |
| 1.49E+00 | 8.37E-01 | -4.59E+00 | -1.12E+00 | -4.28E-01 | 1.41E+00 | 1.26E+00 | 3.61 | 4.80 | 48 | 17300 | 41507 |
| 1.39E+00 | -2.66E-01 | -4.91E+00 | 3.59E-01 | 8.15E+00 | 1.38E+00 | -1.24E+00 | 3.36 | 4.93 | 132 | 16576 | 40899 |
| 3.70E+00 | -1.23E-01 | -1.36E+00 | -7.99E-01 | -7.37E+00 | 1.43E+00 | 1.25E+00 | 8.94 | 1.58 | 49 | 14155 | 11213 |
| 2.11E+00 | 3.22E-01 | -2.37E+00 | -7.58E-01 | -7.18E+00 | 1.44E+00 | -1.27E+00 | 5.09 | 2.51 | 131 | 12752 | 15983 |
| 1.34E+00 | 8.99E-01 | -3.76E+00 | 6.03E-02 | -6.61E+00 | 1.44E+00 | 6.67E-01 | 3.23 | 3.86 | 65 | 12464 | 24075 |
| 8.94E-01 | 7.47E-01 | -4.91E+00 | 5.05E-01 | 3.45E+00 | 1.44E+00 | -1.27E+00 | 2.16 | 4.99 | 131 | 10759 | 26844 |
| 1.13E+00 | -1.45E-01 | -3.78E+00 | -1.05E+00 | 6.16E+00 | 1.44E+00 | 1.26E+00 | 2.72 | 3.92 | 49 | 10663 | 20913 |
| 7.54E-01 | -3.01E+00 | -1.12E+00 | 4.79E+00 | -4.53E+00 | -4.60E-01 | -1.27E+00 | 1.82 | 5.77 | 200 | 10497 | 30283 |
| 6.87E-01 | 8.98E-01 | -5.71E+00 | 1.28E+00 | -6.25E+00 | 1.35E+00 | -1.24E+00 | 1.66 | 5.92 | 133 | 9812 | 29037 |
| 2.07E+00 | -1.28E-01 | -1.74E+00 | -7.39E-01 | 7.44E+00 | 1.44E+00 | 9.37E-01 | 5.00 | 1.89 | 57 | 9465 | 8960 |
| 5.57E-01 | 3.83E-01 | -6.86E+00 | 2.51E-01 | -6.52E+00 | 1.44E+00 | 3.17E-01 | 1.34 | 6.87 | 78 | 9224 | 31690 |
| 8.74E-01 | -3.35E-01 | -4.24E+00 | 5.68E-01 | 2.37E+00 | 1.43E+00 | 1.26E+00 | 2.11 | 4.29 | 49 | 9048 | 19410 |
| 9.32E-01 | 2.94E+00 | 1.74E+00 | -1.89E+00 | 5.64E+00 | 1.42E+00 | 1.22E+00 | 2.25 | 3.90 | 49 | 8771 | 17111 |
| 7.70E-01 | 4.93E-01 | -3.67E+00 | 2.74E+00 | 6.82E+00 | 1.44E+00 | 1.27E+00 | 1.86 | 4.60 | 49 | 8541 | 19649 |
| 8.48E-01 | 1.04E-01 | -3.42E+00 | 2.33E+00 | -2.60E+00 | -1.89E-01 | -1.27E+00 | 2.05 | 4.14 | 188 | 8475 | 17557 |
| 7.71E-01 | 2.36E+00 | -1.86E+00 | -3.35E+00 | 4.80E-01 | 1.44E+00 | -1.08E-01 | 1.86 | 4.50 | 94 | 8374 | 18846 |
| 2.01E+00 | 9.83E-02 | -1.69E+00 | 1.60E-01 | -4.13E+00 | 1.43E+00 | -1.05E+00 | 4.86 | 1.70 | 126 | 8261 | 7028 |
| 3.53E+00 | 4.20E-02 | -8.98E-01 | -2.74E-01 | -2.48E+00 | 1.44E+00 | 1.26E+00 | 8.51 | 0.94 | 49 | 7994 | 3755 |

## DYNAMIC EFFECT OF ROCKFALL ON THE DS/WP

The analyses described here consider the effects of dynamic rock fall on the structural performance of waste packages stored in emplacement drifts at the Yucca Mountain Repository. The rock fall analysis considers a large rock mass that is displaced from the roof of the emplacement drift during a large seismic event. Further, it is assumed for this analysis that this large seismic event occurs at such a time that the drip shield is either missing or is in such a deteriorated state that it offers no resistance to the falling rock mass. The neglect of the drip shield is a significant conservatism. DOE's analysis appears to support a position that the drip shields will survive credible rockfalls for a substantial period of time. Neglecting the drip shield has been done for modeling convenience, to establish an initially conservative analysis of dynamic load. In addition to the conservative neglect of the drip shield, the shape and orientation of the rock mass upon impact and the location of impact on the waste package are assumed to be in a combination that will develop the worst-case damage to the waste package.

The components of the support pallet are assumed to be rigid. Displacement boundary conditions are used to simulate the narrow strips of contact between the support pallet saddles and the exterior surface of the waste package.

The size of the displaced rock is defined to be 7.49 metric tons with a volume of 3.11 $m^3$. This was determined from probabilistic-based rockfall analyses using variations in ground motion records and in situ rock properties (BSC, 2004b). This size of rock is the largest size in a representative grouping considered to have a good probability of occurring for the maximum PGV of 4 m/s associated with a future seismic event. The associated velocity of this rock mass for impact with the waste container was defined to be 4.81 m/s in the rock fall simulations (BSC, 2004b). This is based on the rock mass being ejected from the roof of the emplacement drift during a seismic event having a PGV of 4 m/s (horizontal) as the maximum credible event.

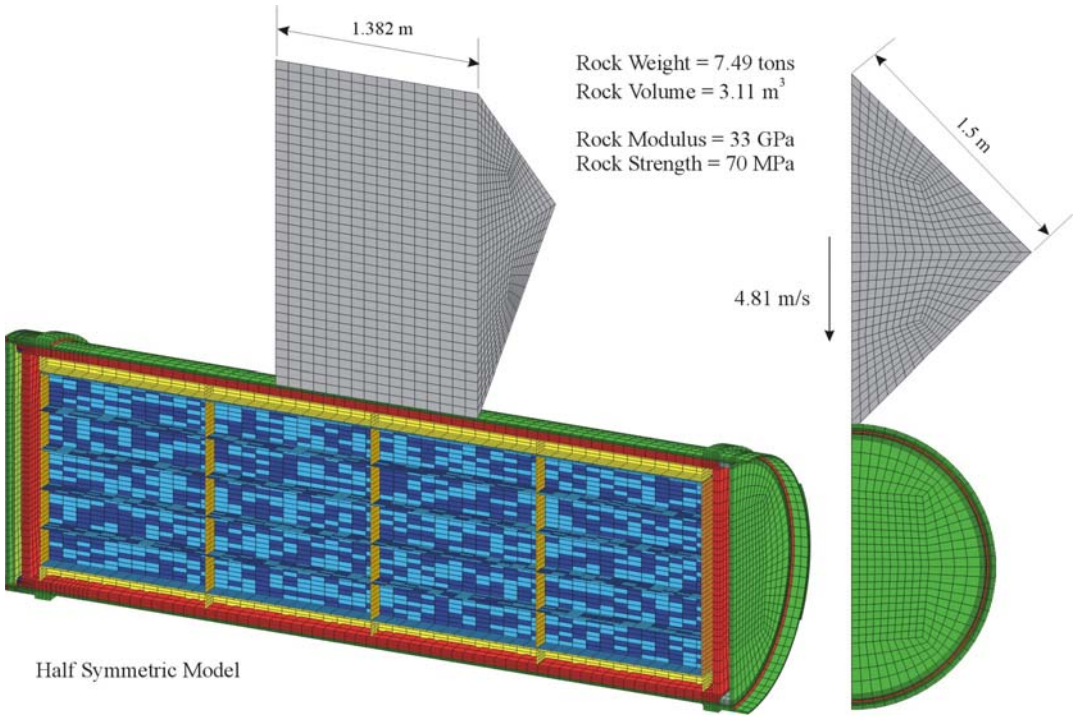


Fig. 2. Finite element model and analysis setup for impact due to rockfall

Fig. 2 illustrates the finite-element approach employed for the analysis of a large rock striking the waste package. The rockfall simulation (BSC, 2004b) for this rock size and mass indicated that the rock would likely strike the drip shield or waste package at an angle, that is, a combination of the horizontal and vertical seismic components would eject the rock from a location that is off-center in the roof. However, for conservatism, the falling rock mass is assumed to strike the waste package directly on the centerline with the velocity vector oriented vertically downward, as illustrated in the figure. This will force the waste package directly into the support skid, which is considered rigid, whereas a strike off-center with some horizontal component of velocity would tend to rock the waste package off the supports. In addition, the rock mass is assumed to be oriented such that it strikes the waste package along an edge of the rock. This is conservative for the container since it focuses the force into a smaller area, as long as the rock does not split into two pieces. The volume of the rock mass is predicted in the rock fall analyses, but the actual shape and dimensions are somewhat arbitrary. A rectangular prism shape is assumed, mainly for ease of modeling as compared to a multi-faceted shape. Two sizes were considered in preliminary runs, the shape shown having 1.5 m square sides and 1.382 m in length, and one having 1 m square sides and 3.11 m in length. The shorter, fatter size shown in the figure was deemed to provide somewhat more damage because it delivers the same impulse load on a smaller area. This rock size was chosen for the final analyses described herein.

The finite element model of the waste package is based on the 21 PWR prototype design and is consistent with other previous analyses for impact with an energetic magma jet (EPRI, 2004c). As in these previous analyses, the model includes fairly detailed representations for the internal basket, guides, and fuel tubes, and smeared modeling for the spent-fuel assemblies. The outer surface of the Alloy 22 outer canister is reduced by 2 mm to consider a somewhat degraded state when the seismic induced rock fall occurs.

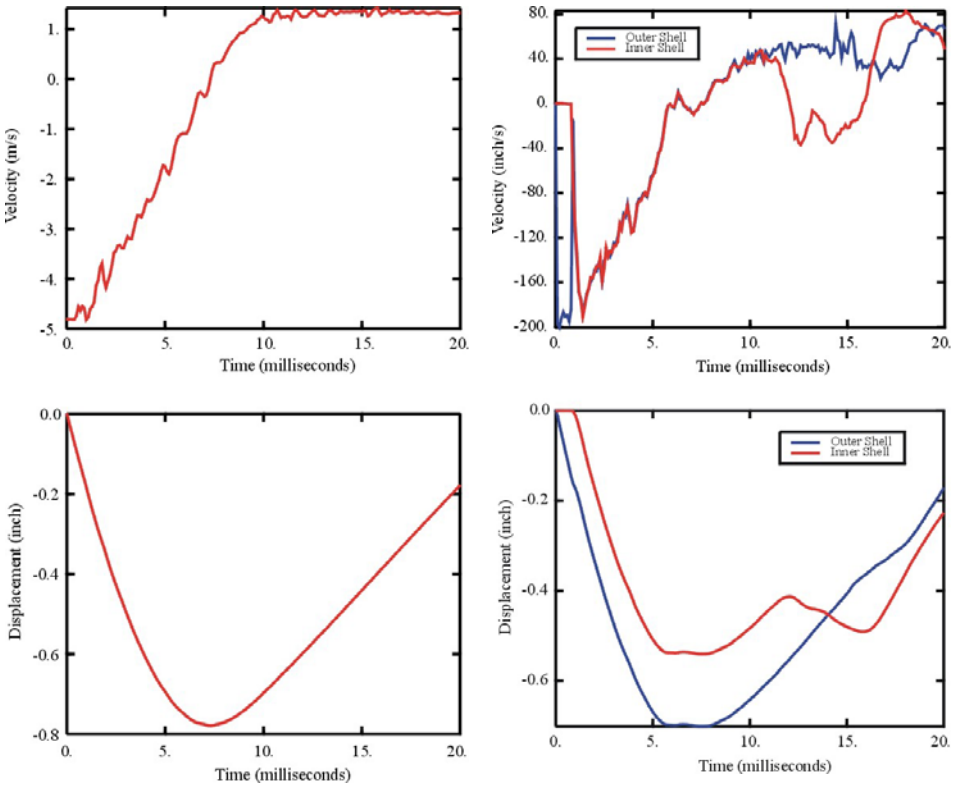


Fig. 3. a) Displacement and velocity histories near the center of the of rock block, b) Displacement and velocity histories of points on inner and outer shell walls of the WP.

The material properties of the waste package components are described in the previous analyses and are evaluated at 80 °C as representative of the long term, steady state temperature in the emplacement drift when the large seismic event leading to rock fall occurs. The properties of the rock mass are taken as follows; Elastic Modulus = 33 GPa (4.785E3 ksi), Poisson's Ratio = 0.18, Compressive Strength = 70 MPa (10.15 ksi), Tensile Strength = 7 MPa (fracture strain = 200E-6). A constitutive model for concrete was adapted and used for the rock. This model allows cracking in tension and assumes elastic, perfectly plastic yielding in compression.

Fig. 3a plots the velocity and displacement histories for points near the center of the rock mass. This figure shows that the momentum of falling rock will be stopped in 7 ms with a total downward displacement of 0.78 inch, and then the rock mass will start to rebound upward. Fig. 3b plots velocity and displacement histories for points on the inner and outer canister walls directly under the impact location. The outer shell reaches a peak deflection of 0.7 inch and the inner shell deflects about 0.55 inch. The gap between the shells close, and then both shells move together until about 10 ms, at which time the inner shell starts to vibrate while the outer shell continues to move outward in contact with the rock mass. There is some slight crushing (or compressive yield) in the rock, mainly near the ends where there is less confinement. The analysis is carried to 20 ms. It can be seen that the rock mass is still moving upward and in contact with the outer shell, but that a secondary impact will be minimal.

Fig. 4a plots a contour for the accumulated equivalent plastic strain in the inner and outer canisters at the end of the analysis. This plot shows that plastic deformation occurs in the inner canister shell wall under the impact, but that the outer canister wall remains elastic in this region. While the outer canister

undergoes more deformation, the stress levels do not reach the yield stress for the Alloy 22 material. Both the inner and outer surfaces of the inner canister shell walls are stressed beyond yield in the area under the knife-edge load. The outer surface yields due to high compressive hoop stress, and the inner surface yields due to high tensile hoop stress. A hard spot at mid-span of the canister due to the locations of the spacer grids in the assemblies and diaphragms in the basket guides creates a double curvature shape in the axial direction and reduces the plastic deformation at the center directly under the load. Fig. 4b shows the plastic strain contours with views from the outside for both the outer canister and the isolated inner canister. This plots shows that some plastic deformation also occurs on the inner canister shell at a cusp location, about 30° from the vertical, from the dishing deformation. This figure also shows some plastic deformation develops on the outer shell at the support locations. This is most likely exacerbated by the rigid support assumption, and in reality, the support structure will deform slightly under the impact loading and spread the reaction force over a larger area on the outer shell surface.

From these results, it is concluded that a rock fall impact event with the given size, mass, and velocity of the rock mass will have very little effect on the longevity of the Alloy 22 protective canister. The response of the Alloy 22 material under the impact will likely remain in the linear regime, even with some corrosive thickness reduction, and thus, residual stresses that could accelerate the degradation from stress corrosion cracking will not be present. It seems especially evident that if residual stresses near the yield strength of the material are needed for stress corrosion cracking, then such a rock fall event will most certainly not affect the performance or longevity of the waste package.

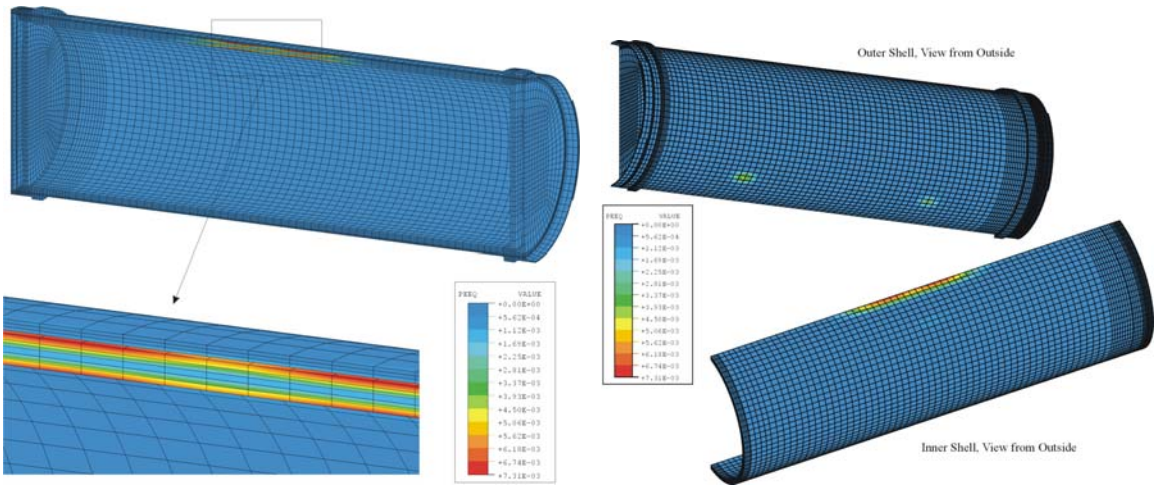


Fig. 4. a) Contour of equivalent plastic strains, b) Backside views of plastic strain for inner and outer canister shells

## CONCLUSION

Yucca Mountain is located in the somewhat seismically active Basin and Range province. Future seismic activity is identified by the US Nuclear Regulatory Commission and the US National Academy of Sciences as a key scenario for safety assessment of a proposed repository at Yucca Mountain. As part of its on-going program of conducting independent analyses of scientific and technical issues that could be important to the licensing of the Yucca Mountain repository, EPRI has conducted an analysis of the combined scenarios of seismic activity and stability of emplacement drifts with respect to the long-term repository safety. In this paper we present the results of 3D finite element simulations of both static and dynamic loading of a degraded waste package. For the static case, the expected maximum static load is

determined by utilizing relationships between cave height and the bulking factor. A static load representing 30 meters of broken rock was simulated using the finite element model. For the dynamic case, block size and velocity data from the most recent Drift Degradation AMR are used. Based on this, a rock block with a volume of 3.11 $m^3$ and with an impact velocity of 4.81 m/s was simulated using the finite element model. In both cases, the results indicate that the waste package remains intact.

## REFERENCES


1. Abaqus, 2005. ABAQUS/Explicit, Version 5.8, ABAQUS, Inc (formerly Hibbitt, Karlsson, and Sorensen, Inc.) Pawtucket, R.I., www.abaqus.com.
2. BSC, 2004b. (Bechtel SAIC Company), Drift Degradation Analysis, Bechtel SAIC Company report to DOE ANL-EBS-MD-000027, REV 03, ICN 00. Las Vegas, Nevada. ACC: MOL.20040513.0081.
3. Bell, F.G.; Stacey, R. 1992: Subsidence in Rock Masses. Ch 13 of Engineering Masses. Butterworth-Heinemann.
4. Blyth, F.G.H.; de Freitas, M.H. 1990: A Geology for Engineers. Edward Arnold.
5. Church, H.K. 1981: Excavation Handbook McGraw-Hill International Book McGraw-Hill International Book Company.
6. Dyne, L. A. (1998). The Prediction and Occurrence Of Chimney Subsidence Southwestern Pennsylvania. Master Of Science Thesis, Virginia Polytechnic and State University, Dept. Mining and Minerals Engineering, Blacksburg,
7. EPRI, 2004a. Evaluation of a Spent Fuel Repository at Yucca Mountain, Report: Interim Report, September 2004. EPRI Technical Report 1009705, Research Institute, Palo Alto, CA.
8. EPRI, 2004b. Comments Regarding In-Drift Chemistry Related to Corrosion Barriers at the Candidate Spent Fuel and HLW Repository at Yucca Mountain, Technical Report 1010941. Electric Power Research Institute, Palo Alto, Potential igneous processes relevant to the Yucca Mountain repository: scenario. EPRI Technical Report 1008169. Electric Power Research
9. EPRI, 2005a. Program on Technology Innovation: Potential Igneous Yucca Mountain Repository: Intrusive-Release Scenario: Analysis and Technical Report 101165. Electric Power Research Institute, Palo Alto,
10. EPRI, 2005b. Yucca Mountain Licensing Standard Options for Very Technical Bases for the Standard and Compliance Assessments, Interim Report 1011754. Electric Power Research Institute, Palo Alto, CA.
11. EPRI, 2005c. Effects of Seismicity and Rockfall on Long-Term Performance of the Yucca Mountain Repository, Progress Report 1011812, Electric Power Research Institute, Palo Alto, CA.
12. Gute, G.D., G. Ofoegbu, F. Thomassy, S. Hsiung, G. Adams, A. Ghosh, B. Dasgupta, A.H. Chowdhury, and S. Mohanty. "MECHFAIL: A Total-system Performance Assessment Code Module for Evaluating Engineered Barrier Performance under Mechanical Loading Conditions." CNWRA 2003–06. San Antonio, Texas: CNWRA. 2003.
13. NRC, 2005. RISK ANALYSIS FOR RISK INSIGHTS PROGRESS REPORT Prepared for U.S. Nuclear Regulatory Commission, Prepared by S. Mohanty, R. Benke, R. Codell, 1 K. Compton,1 D. Esh,1 D. Gute, L. Howard, T. McCartin, 1 O. Pensado, M. Smith, G. Adams, T. Ahn,1 P. Bertetti, L. Browning, G. Cragnolino, D. Dunn, R. Fedors, B. Hill, D. Hooper, P. LaPlante, B. Leslie, 1 R. Nes, G. Ofoegbu, R. Pabalan, R. Rice, 2 J. Rubenstone,1 J. Trapp,1 B. Winfrey, L. Yang 1U.S. Nuclear Regulatory Commission 2Consultant Center for Nuclear Waste Regulatory Analyses San Antonio, Texas May 2005.
14. Palchik, V. (2001) Influence of physical characteristics of weak rock mass caved zone over abandoned subsurface coal mines. *Environmental Geology* – 101.
15. Singh, K. B. and B. B. Dhar (1997). Sinkhole subsidence due to mining *Geotechnical and Geological Engineering*, 1997, **15**, 327–341
16. Whittaker, B.N.; Reddish, D.J. 1993: Subsidence Behaviour of Rock Structures. Vol 4 of Comprehensive Rock Engineering. Pergamon Press, 1993.